



# Surface Modification of a Cold Gas Dynamic Spray-Deposited Titanium Coating on Aluminum Alloy by using Friction-Stir Processing

F. Khodabakhshi<sup>1</sup> · B. Marzbanrad<sup>2</sup> · L. H. Shah<sup>3</sup> · H. Jahed<sup>2</sup> · A. P. Gerlich<sup>2</sup>

Submitted: 7 January 2019 / in revised form: 24 April 2019 / Published online: 14 August 2019  
© ASM International 2019

**Abstract** In this research, the parameters of the cold spray process were initially assessed for deposition of a pure titanium coating layer with the thickness in the range of 800–850  $\mu\text{m}$  on an AA5083 alloy substrate. Thereafter, to enhance the structural integrity of Ti-coating layer and decrease the coating porosity, friction-stir processing was employed as a post-modification technique by using a flat cylindrical tungsten carbide tool. The plunge depth of the friction-stir tool (in the range of 0.3–0.5 mm) was found to significantly affect the densification of the porous titanium coating layer. Optical microscopy, field emission-scanning electron microscopy, electron backscattering diffraction, transmission electron microscopy analysis and indentation Vickers micro-hardness testing were conducted on the thickness cross-sections of cold-sprayed coatings to characterize the microstructural features and mechanical properties before and after friction-stir modification performed using two different plunge depths. Furthermore, residual stress profiles on the surface were determined by using x-ray diffraction analysis technique. Significant grain refinement, from an initial cold-sprayed coating grain size

of less than 25  $\mu\text{m}$  to grain sizes  $< 1 \mu\text{m}$ , was observed across the thickness section of modified samples with a gradient profile from the coating surface toward the interface depending on the plunge depth. After friction-stir processing, the hardness of a thin layer close to the surface of coating increased up to seven times higher as compared to the cold-sprayed material.

**Keywords** AA5083 alloy substrate · cold spray · friction-stir processing · hardness · microstructure · Ti-coating

## Introduction

Cold spray (CS) or in general cold gas dynamic spray (CGDS) is well developed as a promising and novel technology to coat the surface of different metals and alloys with different materials by using the high-velocity impact mechanism to attain an improvement in several physical and mechanical characteristics (Ref 1). However, some disadvantages may restrict the application of CS coating (Ref 2). During high-velocity impact, the semi-spherical morphology of particles can cause the formation of porosities between deposited particles (Ref 3). Formation of a high dislocation density during impingement, heterogeneous grain structure, and poor interfacial adhesion/bonding are the other main concerns (Ref 3, 4), since these features can have a detrimental influence on mechanical performance (Ref 1). Therefore, to enhance the integrity and homogeneity of coatings, and improve the metallurgical bonding strength between coating and substrate, implementation of a post-spray treatment offers many benefits (Ref 1, 5). It is obvious that by applying a simple post-annealing heat treatment to the CSed coatings, the coating microstructure can be partly homogenized,

---

**Electronic supplementary material** The online version of this article (<https://doi.org/10.1007/s11666-019-00902-z>) contains supplementary material, which is available to authorized users.

---

✉ F. Khodabakhshi  
farzadkhodabakhshi83@gmail.com; fkhodabakhshi@ut.ac.ir

- <sup>1</sup> School of Metallurgical and Materials Engineering, College of Engineering, University of Tehran, P.O. Box 11155-4563, Tehran, Iran
- <sup>2</sup> Department of Mechanical and Mechatronics Engineering, University of Waterloo, Waterloo, ON, Canada
- <sup>3</sup> Faculty of Mechanical and Manufacturing Engineering, Universiti Malaysia Pahang, 26600 Pekan, Pahang, Malaysia

which is driven by the mechanism of solid-state atomic inter-diffusion, and leads to improved cohesion bonding at the interface (Ref 6, 7). Meanwhile, mechanical properties may not improve noticeably due to limitations in reducing the pore fraction by diffusion phenomenon, along with potential coarsening of precipitates and grains due to thermal annealing (Ref 7). Therefore, development of another new complementary solid-state post-modification technique to attain a dense CS coating with a uniform ultra-fine-grained structure is highly appropriate since this can further enhance mechanical strength.

For structural and industrial applications, an appropriate combination of different mechanical properties as well as varying degrees of processing freedom is required. One innovative adaptation surface modification methodology is based on friction-stir processing (FSP) (Ref 8). During FSP process, a non-consumable rotating tool is plunged downward to generate the frictional heating contact, and thereafter by translating along the contact/modification line, plastic material flow occurs at a temperature below the melting point, while material is transferred from the leading edge to trailing side, leading to the formation of a stirred region (Ref 9, 10). It is well accepted that the formation of a fine or ultra-fine equiaxed grain structure during FSP of metals and alloy is attributed primarily to the dynamic restoration phenomena associated with thermo-mechanical treatment (Ref 11, 12).

One of the interesting applications of FSP can be to apply for modification of the structure of porous coatings manufactured by CS process and mitigate the related issues, although there is limited research focused on this. In the first attempt by Hodder et al. (Ref 13), it is demonstrated that Al-Al<sub>2</sub>O<sub>3</sub> metal matrix composites can be deposited on the surface of an AA6061 aluminum alloy substrate by the low-pressure CS process, and thereafter modified by using FSP. A hardness increase of up to ~ 60% was attained after FSP owing to densification of the coating layer and a more uniform distribution of alumina particles (Ref 13). In another work by Ashrafizadeh et al. (Ref 14), FSP was employed to modify the tungsten carbide (WC)-based metal matrix composite coating layer deposited by the low-pressure CS process on a low-carbon steel substrate. Considerable improvements in hardness and wear resistance of the coating layer were reported after FSP compared to the as-sprayed materials (Ref 14). In a study by Huang et al. (Ref 15), AA5056-SiC metal matrix composites were deposited on the surface of pure aluminum substrate and then modified by FSP. The main focus was on improving the tribological properties of coating layer as caused by the hot consolidation effect during FSP, producing a uniform dispersion of particles with considerable microstructural refinement (Ref 15). A two times improvement in hardness was noted for the FSP-

modified coating as well as a higher friction coefficient. The same composite system was also applied onto an AA2024 aluminum alloy substrate by a hybrid implementation of CS and FSP methods (Ref 16). It was found that the combination of a reduction in porosity, particle fragmentation, and grain structural refinement led to a softening trend in the hardness profiles of FSP-modified coating for that case (Ref 16). Different coating compositions of WC-CoCr, Cr<sub>3</sub>C<sub>2</sub>-NiCr, and Al<sub>2</sub>O<sub>3</sub> were deposited on an AA5083 alloy substrate and thereafter modified by using a spray-stirring route (FSP and CS) in a broad study by Peat et al. (Ref 17, 18). The main aim was improving the erosion performance (Ref 18). With a coating thickness drop of ~ 40%, a hardness improvement of up to ~ 540% was reported for the optimal parameters (Ref 17). In a research by Huang et al. (Ref 19), an ultra-fine-grained high-strength thick-coating of brass was fabricated by a combined subsequent accomplishment of CS and FSP processes (Ref 19). Characterization results showed a noteworthy tensile strength increasing up to three times higher as compared to the as-sprayed material, along with an elongation enhancement of ~ 400% (Ref 19).

In a recent study by the present authors (Ref 20), an AA7075 aluminum alloy coating layer was deposited on the surface of an AZ31B magnesium alloy substrate and then friction-stir-modified. Significant improvements in the hardness of coating layer and substrate were noted as up to ~ 80 and 30%, respectively, in correlation with the related induced grain structural refinements. Another research by current researchers showed the formation of interfacial chemical bonding between aluminum and titanium during CS deposition and subsequent FSP modification by implementing the electron microscopy analysis (Ref 21). In follow-up studies, CS process was used in the current research to initially deposit pure titanium particles on the surface of an AA5083 alloy substrate. Thereafter, modification of the coating structure was achieved by single-pass FSP. The outputs of the present research can be relevant to specific industrial applications in the biomedical, aeronautical and automotive industries. The effects of tool plunge depth as the main FSP controlling parameter on the microstructural characteristics and mechanical properties of CSed coating layer before and after modification were investigated. X-ray diffraction (XRD) analysis technique was performed for the aim of residual stress measurements and accordingly the results discussed based on developments in the microstructural features. Also, this research can be continued in the future by evaluating the influence of surface hardening and compressive residual stress build-up on the fatigue performance of FSP-modified CSed Ti-coating.

## Experimental Methodology

### Materials

The non-heat treatable AA5083 (aluminum-magnesium) alloy substrate with a thickness of 10 mm, a nominal chemical composition of Al-4.5Mg-0.7Zn-0.85Mn-0.11Fe-0.08Si-0.015Ti (wt.%), and in the H34 initial temper was supplied and utilized as the substrate. It was machined to the small samples with surface plane dimensions of 100 mm × 100 mm before application. Also, pure titanium powder with spherical morphology of particles and average size of ~ 63 μm was ordered from TLS Technik GmbH & Company (Ti Gd2, Spezialpulver KG, Germany) and used as the coating material. Details for morphology and size distribution of titanium particles are shown in FE-SEM images of Fig. 1.

### Cold Spray Deposition

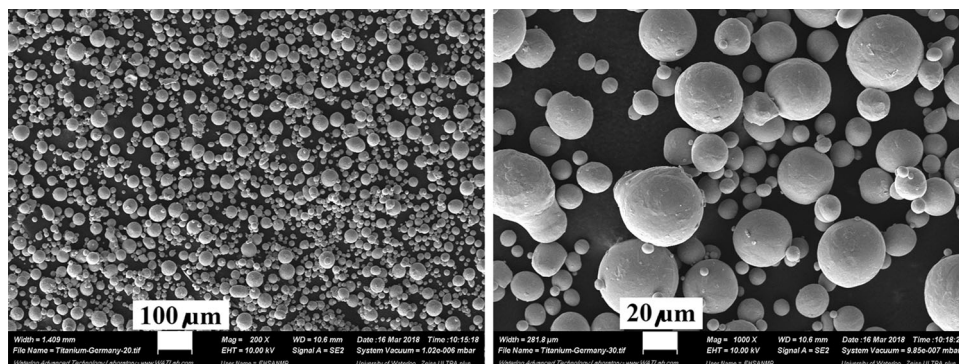
To improve the bonding between Ti-coating and AA5083 alloy substrate, the surface of substrate was ground before spraying and then cleaned by ultrasonic vibration in the acetone and ethanol baths. Deposition of titanium powder on the AA5083 alloy substrate was performed by using a low-pressure CS system of SST series model P manufactured by the CenterLine Company (CenterLine Co., Windsor, Ontario, Canada), connected with a series 4000 volumetric powder feeder (5MPE, Oerlikon Metco, Westbury, NY, USA) using nitrogen as carrier gas to transport the powder from storage to nozzle. In the design of this machine, a commercial CS gun with a converging–diverging de Laval UltiLife™ nozzle with a length of 120 mm, orifice diameter of 2 mm, and exit diameter of 6.3 mm was mounted on a robotic arm (HP-20, Motoman, Yaskawa Electric Corp., Waukegan, IL, USA) for automatic controlling and to enhance the repeatability of coating depositions. High-pressure compressed nitrogen gas was used as carrier gas to accelerate the titanium powder particles. Also, the other conditions and parameters

used during CS process to produce a layer of Ti-coating with the thickness in the range of 800–850 μm were found as follows. The criteria for this evaluation involved varying the processing parameters to reach a good deposition of titanium on the AA5083 substrate with a sound surface appearance. The inlet pressure and temperature of nitrogen gas as the working fluid were determined as 1.42 MPa (203 psi) and 500 °C, respectively, with a feeding rate of 7 rpm (2.24 g/min). The stand-off distance between the substrate and nozzle exit was kept constant about 30 mm. For CS deposition, a surface with dimensions of 40 mm × 100 mm was covered with the transverse hatches (overlapped layer beside of layer deposition along the transverse direction) by setting the gun traverse velocity to 2.5 mm/s and step over of 2.5 mm. A top-view image from the surface of processed sample (AA5083 alloy substrate coated with a titanium layer) is presented in Fig. 2(a). Based on preliminary testing and examinations, the other ranges of CS processing parameters from the highlighted working window defined earlier could not provide better Ti-coatings with improved surface appearance or integrity.

### Modification by Friction-Stir Processing

In the next step, the produced CS coating layer was modified by FSP process. A single FSP pass was accomplished parallel to the longitudinal direction of substrate by using a high-power displacement-controlled 7.5-HP spindle vertical commercial milling machine (Jafo Manual Universal Milling Machine, Manchester, England). To minimize the chemical reactions between FSP tool and Ti-coating, a tungsten carbide (WC) pin-less simple cylindrical tool with the shoulder diameter of 12 mm was used. Various processing parameters were assessed by FSP modification to identify a suitable working window which avoided excessive vibrations. After some iterative trials, FSP process was conducted on the main CSed sample along the length by keeping a constant tool tilting angle of 2.5° with respect to the substrate plane to prevent from chipping of Ti-coating. Also, the main FSP parameters were controlled as tool

**Fig. 1** FE-SEM images from the titanium particles at two different magnifications



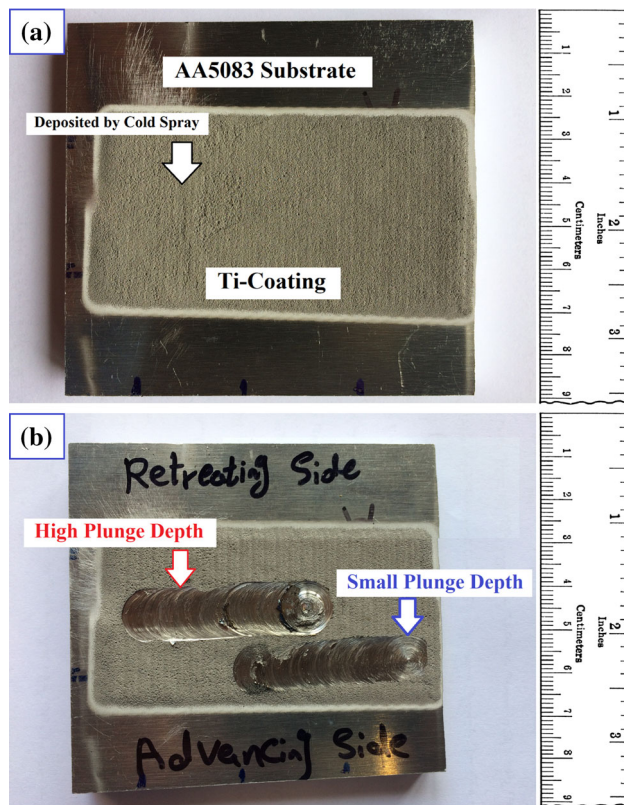


**Fig. 2** (a) The CS-deposited AA5083-Ti sample. (b) FSP modification on the cold-sprayed titanium layer at two different plunge depths

rotational speed ( $\omega$ ) of 900 rpm and traverse velocity ( $v$ ) of 63 mm/min with a clockwise direction of rotating tool. As highlighted in previous studies (Ref 13, 20), the tool plunge depth has a significant influence on the modification of CSed coatings by using FSP. Therefore, two different plunge depths (0.3 mm as low, and 0.5 mm as high) of FSP tool into the Ti-coating were tested in this work to study their related developments. Figure 2(b) shows the image from friction-stir-modified CSed coatings with small and high tool plunge depths. Images demonstrating the experimental accomplishment of these high and low plunge depth steps of FSP modification on the CSed Ti-coating are shown in Electronic Supporting Information (ESI) Figs. S1a and S1b, respectively.

### Microstructural Characteristics

The specimens processed with low (0.3 mm) and high plunge depths (0.5 mm) were cross-sectioned perpendicular to the FSP direction by using a diamond cutter. The thickness section across the FSP direction was examined for further microstructural studies. After standard metallographic sample preparation procedures by mechanical grinding and polishing on diamond pastes down to 0.1  $\mu\text{m}$ , the microstructure of substrate and coating layer was

revealed by a two-step chemical etching process. At first, etching of AA5083 alloy substrate was performed by using a modified Poulton's reagent (a mixture of 1 ml  $\text{H}_2\text{O}$ -6 ml  $\text{HNO}_3$ -1 ml  $\text{HF}$ -12 ml  $\text{HCl}$  and 25 ml  $\text{HNO}_3$ -1 g  $\text{H}_2\text{CrO}_4$ -10 ml  $\text{H}_2\text{O}$  solutions) for about 5-10 s. To etch the Ti-coating layer, mechanical polishing of surface was continued by vibratory polishing on the colloidal silica ( $\text{SiO}_2$ ) suspension with the average particle size of 20 nm for about 45 min. Then, chemical etching was performed by using a commercial Kroll's reagent (distilled water-nitric acid-hydrofluoric acid) for about 5 s. Macro-patterns of material flow were observed under a Nikon stereographic microscope (Nikon, USA). An Olympus optical microscope (OM, Olympus PME3, Germany) was used for the aim of microstructural observations. The average grain size was measured using the standard linear intercept method described in ASTM E112. To study the structural developments in Ti-coating layer before and after CS and FSP processes, the polished metallographic samples before chemical etching were examined under a field emission-scanning electron microscope (FE-SEM, Zeiss Leo 1530, ZEISS, Germany) equipped with an energy-dispersive x-ray spectroscopy detector/orientation imaging microscopy (EDX/OIM). The fraction of porosities within the deposited coating layer before and after FSP modification was estimated by image analysis for at least 20 cross-sectional FE-SEM micrographs. After performing broad ion-milling on the titanium coating layer, its grain structure was studied under FE-SEM microscope using the channeling contrast concept. More details characterizations on the grain structure of titanium coating layer after FSP treatment were performed by using transmission electron microscopy (TEM) analysis.

### Indentation Hardness

Mechanical property of CS-deposited Ti-coating layer before and after FSP modification was assessed in the terms of indentation hardness testing from different regions across the thickness section of processed samples. These Vickers micro-indentation hardness measurements were performed according to "ASTM E384-17" Standard Test Method (Ref 22). The AA5083 alloy substrate, CSed Ti-coating, and different locations (advancing side, center line, retreating side, and Al/Ti interfaces) of low and high plunge depth FSP-modified coatings were evaluated by Vickers hardness indentation perpendicular to the FSP line. These measurements were performed using a Buehler Vickers micro-hardness indenter (Buehler, Germany) with an applied load of 300 g and dwell time of 15 s. The hardness results were reported in the optical images from the indentation features, with the Vickers micro-hardness values indicated at each indent location.

## Results and Discussion

### Cold Spray Deposition of Ti-Coating on the AA5083 Alloy Substrate

FE-SEM images from the structure of deposited Ti-coating on the AA5083 alloy substrate are presented in Fig. 3 (before chemical etching). The coating structure appears porous, where the fraction of porosity was calculated by image analysis to be ~ 30%. Furthermore, it seems that with increasing distance from Al/Ti interface the coating structure became more porous in the layers close to top surface. This heterogeneous trend of pore formation is related to the layer-by-layer deposition of material and the gradual decrease in effective surface for deposition by shifting from the interface toward the top surface layer. The interface morphology between the as-sprayed coating and substrate exhibits a wavy pattern. This wavy interface is common during cold spray deposition and similar to explosive welding process, but in a microscale here. The EDS elemental mapping analysis results from Al-Ti bimetallic structure produced by CS are shown in Fig. 4. As expected, considering the low deposition time and moderate inlet gas preheating temperatures during the CS process, there is no significant large-scale inter-diffusion between Al, Mg and Ti elements at the bonding interface.

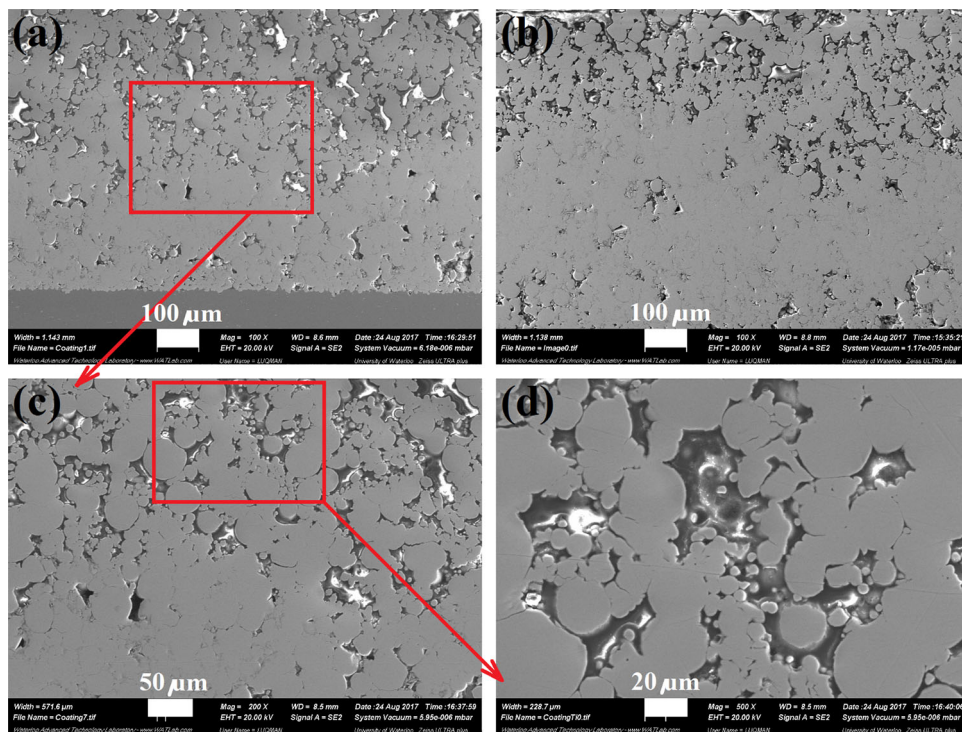
### Effects of FSP Process with Two Different Plunge Depths on Material Flow

In Fig. 5(a) and (b), influence of FSP modification at low (~ 0.3 mm) and high plunge depths (~ 0.5 mm) on the materials flow pattern for the CSed coating layer around the shoulder-affected zone is illustrated with presentation and combination of some stereographic and optical micrographs. The considerable influence of FSP on densification of porous the Ti-coating in both the low and high plunge depth processing conditions can be noted, due to the forging action and deformation imposed by the tool (Ref 9, 10, 23). This densification affect appears to be more intense under the high plunge depth forging condition, as supported by close-up view in high-magnification images in Fig. 5(b).

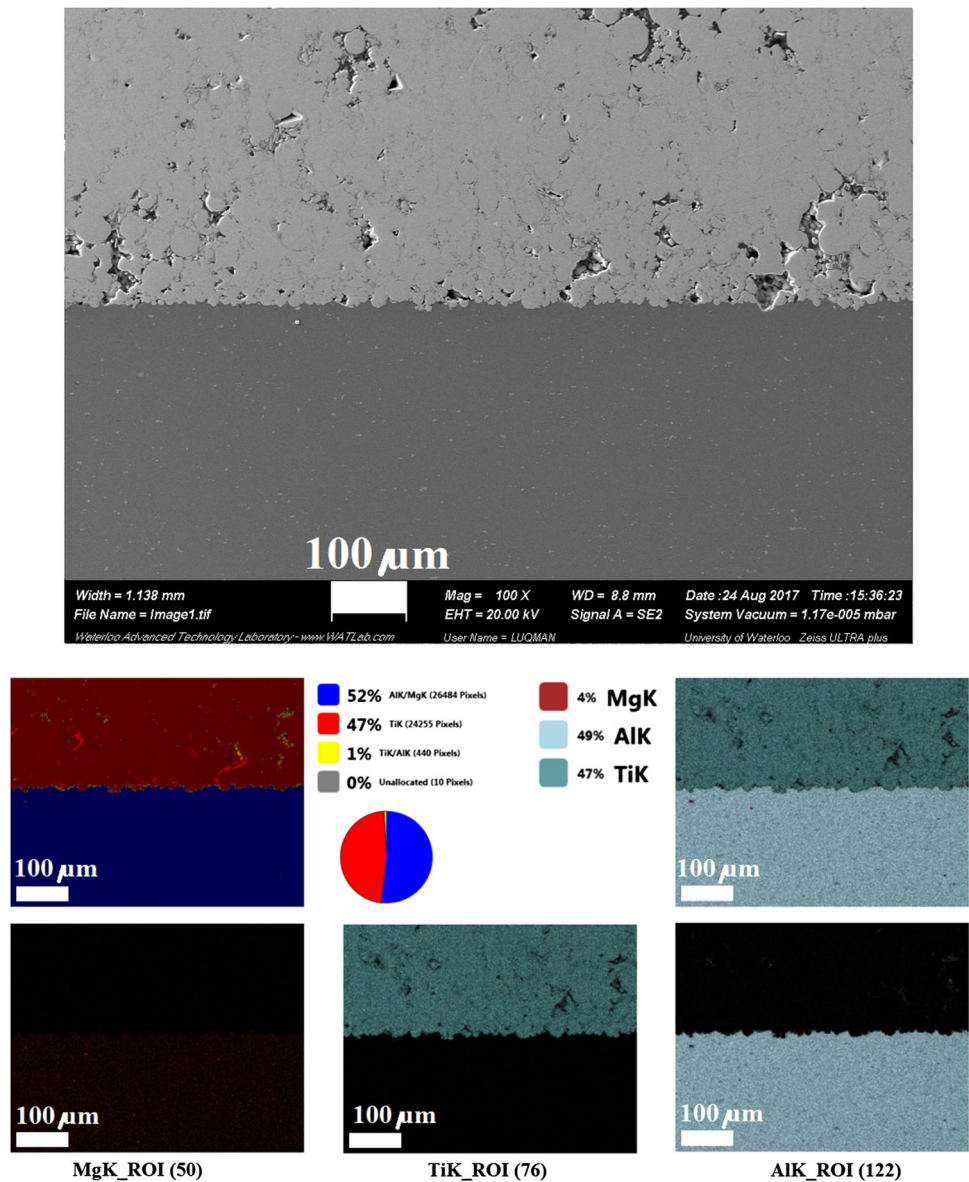
### Grain Structural Evolution

Optical grain structures from the thickness center and surface sections for initial AA5083 alloy substrate are shown in ESI Figs. S2a and S2b, respectively. An elongated and an equiaxed grain structures are seen for the thickness and surface cross-sections of as-received substrate, respectively. In Fig. 6(a) and (b), optical micrographs from the grain structure of the CS-deposited Ti-coating layer after chemical etching reveal the grain

**Fig. 3** FE-SEM images from the structure of CSed Ti-coating



**Fig. 4** An FE-SEM image combined with the elemental mapping analysis results from the interface of CSed Ti-coating with the AA5083 alloy substrate



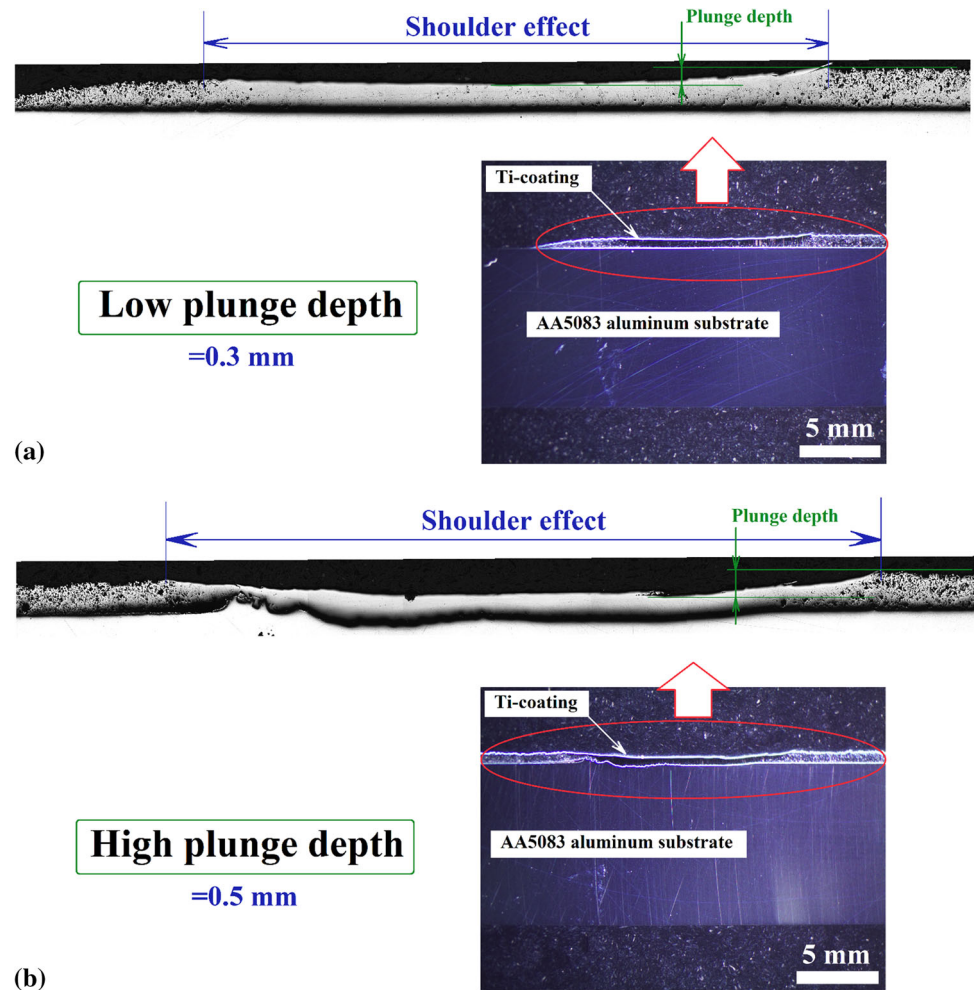
structure as well as the particle boundaries consists of a globular morphology with an average size of lower than  $25\ \mu\text{m}$ . Since both of grain and particle boundaries are simultaneously etched for Ti-coating by using Kroll's reagent, and the particle boundary coincides with a grain boundary as well, the reported mean grain size values in this section and onwards represent an average contributed from both of these factors.

Figure 6(c), (d) and (e), (f) demonstrates the effects of low and high plunge depth FSP modifications on the grain structure of Ti-coating layer, respectively. For the low plunge depth sample, the grain structure of the coating close to the interface is the same as the as-deposited CS one, although with a lower fraction of porosity due to densification imposed by the forging action of the rotating tool. Meanwhile, the grain structure is gradually more

refined toward the top surface layer (see Fig. 6c, d). A thin layer on the surface with a very fine structure and different morphology or contrast is visible. It is difficult to estimate the accurate mean grain size for this thin layer on the surface. However, at high-magnification optical micro-images suggest that this layer is finer than one micron. For the high plunge depth sample, the thickness of this fine-grained layer is considerably deeper with a different material flow pattern due to the more aggressive forging action and severity of tool stirring. In addition, the globular microstructure near interface is refined more considerably compared to the low plunge depth specimen, with a corresponding reduction in porosity as well.

In the case of Ti-coating, studying the microstructural features with more details revealed very interesting aspects as presented in Fig. 7 and 8. FE-SEM images from Ti-

**Fig. 5** Stereographic macro-profiles from the thickness cross-sections of modified Ti-coatings by FSP at (a) low and (b) high plunge depths as combined with the related optical micro-images



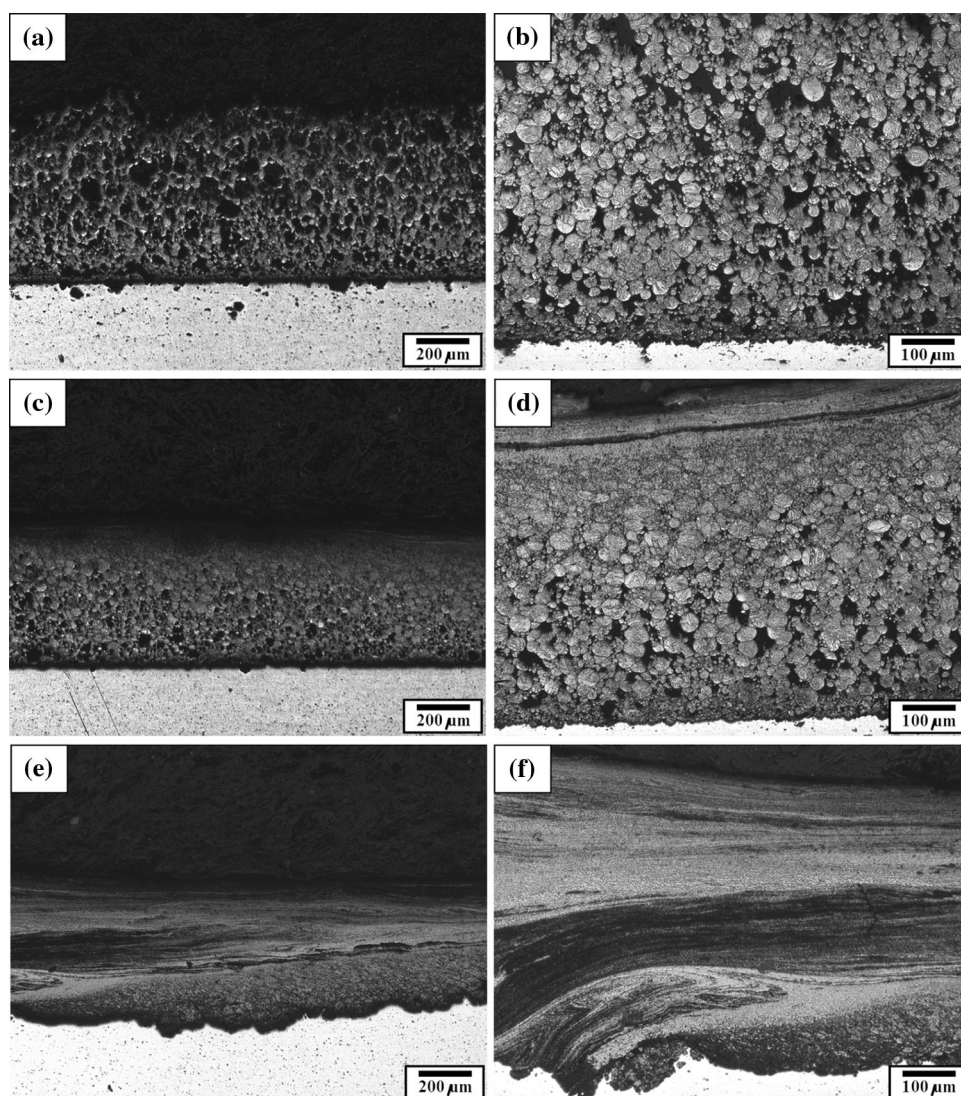
coating after ion-milling in Fig. 7 demonstrate a grain structure elongated perpendicular to the deposition direction in the micron scale by channeling contrast observation. Further characterization of modified titanium coating close to its interface with aluminum substrate by TEM analysis is illustrated in Fig. 8. Formation of a sub-grain structure from ultra-fine grains with average size of less than 500 nm can be noted caused by high strain rate intense plastic deformation of CS deposition and subsequent friction-stirring step. By considering the stacking fault energy and microstructure of the examined AA5083 alloy substrate and pure Ti-coating, discontinuous dynamic recrystallization (DDRX) assisted by dynamic recovery (DRV) has been cited as the main operative mechanisms during FSP of these alloys in prior work (Ref 24, 25). As reported in the literature (Ref 26, 27), the maximum temperature of the stir zone during FSP of pure titanium is generally higher than the  $\alpha$  to  $\beta$  titanium phase transition temperature ( $\sim 882$  °C). This implies that the hot deformation process followed by forging and consolidation usually occurs in the  $\beta$  phase crystal structure. Therefore, observation of this different layer on the surface with an equiaxed morphology

of grains can reveal transformation of sub-structure to  $\alpha'$ -Ti lath- and lens-martensite ( $\beta$  to  $\alpha'$  transformation) structure after the dynamic recrystallization phenomenon (Ref 25, 27).

### Microstructural Developments During FSP Modification

Combined FE-SEM images showing the material flow patterns across the thickness section of the low and high plunge depth friction-stir-modified Ti-coatings are presented in Fig. 9(a) and (b), where evidence of considerable densification and homogenization can be seen in these macrographs. As seen, the thickness of the CSed Ti-coating varied from 800 to 850  $\mu\text{m}$ . High-magnification FE-SEM images from the structure of modified CS coating with low plunge depth at different regions are shown in Fig. 9(a). It can be found that the structure of the coating close to surface section became fully dense due to the effect of the forging imposed by the FSP tool; however, a fraction of porosity and inhomogeneities still remain at the Al/Ti interface. In the FE-SEM images from the high plunge

**Fig. 6** Optical grain structures of (a, b) as-sprayed Ti-coating, and modified ones after FSP by (c, d) low and (e, f) high plunge depths, at two different magnifications



depth FSP specimen (shown in Fig. 9b), full densification is evident in the regions close to the Al/Ti interface. Also, some complex materials flow patterns are visible on the surface layer. Furthermore, the macro- and micro-locking morphologies at the interface are completely different from the low plunge depth sample with a long and fine wavy pattern. During these FSP modification steps, no shielding gas was used for protection. Therefore, exposure to the atmosphere can affect the structure of the hot surface layer after it emerges from under the rotating shoulder during frictional heating and severe plastic deformation. Oxygen and nitrogen exhibit high affinities for titanium in the solid solution as interstitials which played role as  $\alpha$ -stabilizer elements (Ref 26). Thus, these will accelerate the  $\beta$  to  $\alpha'$  phase transformation to produce martensite upon cooling from high temperature after FSP modification. In XRD pattern from the surface of FSP-modified Ti-coating as shown in Fig. 10, the presence of some retained  $\beta$ -phase

upon transformation to room temperature is noticeable as well as the titanium oxide phase.

This chemical adsorption process for trapping or binding of  $O_2$  and  $N_2$  elements occurs by hot severe plastic mixing during FSP process and exposing the surface plasticized material to the atmosphere (Ref 27). Consequently, pickup of elements can be accelerated by their strong affinity of titanium with oxygen and nitrogen elements (Ref 25). Therefore, the driving force for this adsorption phenomenon can be exothermic in nature similar to nitriding and oxidation processes (Ref 25, 27). By continuing the FSP process along with gradual exposure of the processed material to the atmosphere, solid-state diffusion will play an important role in the formation of a hardened surface layer. Since the diffusion is a rate-controlling phenomenon as a function of temperature and time, higher maximum temperature with more exposure or dwell time can accelerate this process (Ref 25, 27). Due to grain structural



**Fig. 7** Channeling contrast FE-SEM images from the grain structure of FSP-modified Ti-coating after ion-milling and etching

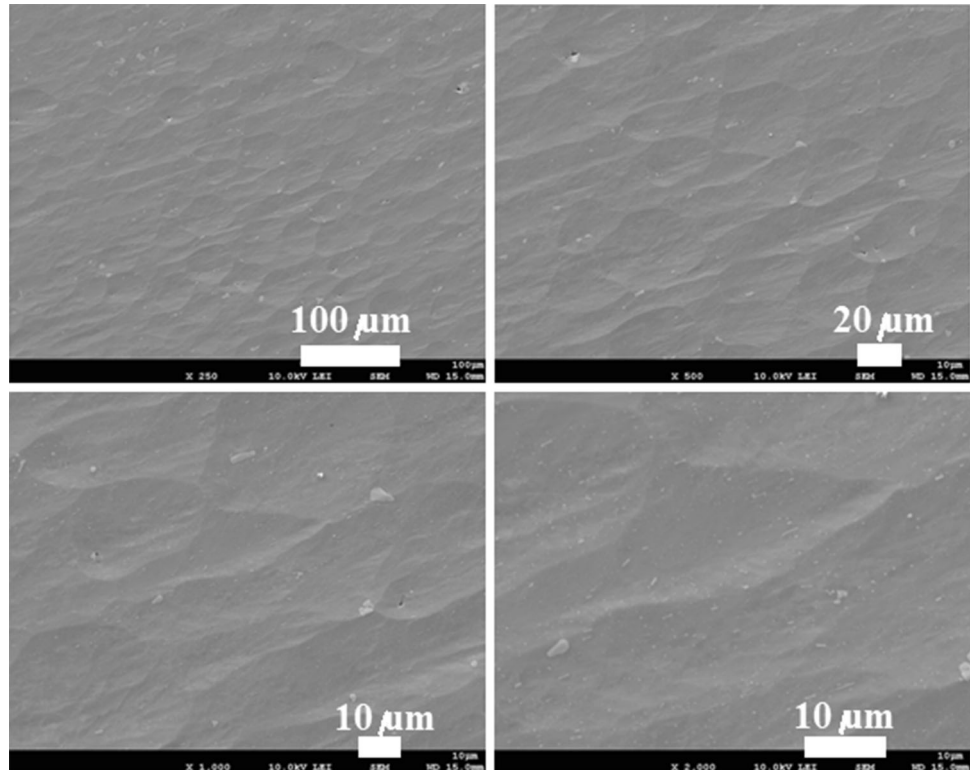
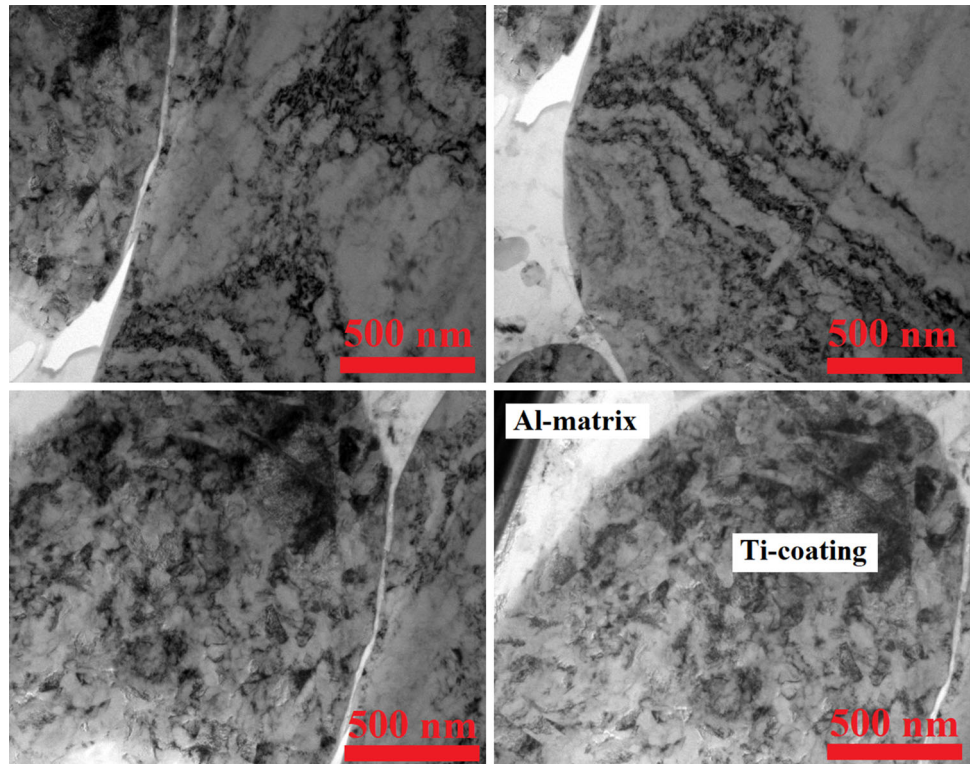


**Fig. 8** TEM images showing the sub-grain structure of Ti-coating close to the interface with aluminum substrate for high plunge depth sample



refinement during FSP leading to an increase in the fraction of grain boundaries, interstitial diffusion of N and O elements within the structure of the processed titanium surface

will increase. It is also possible for Ti/titanium oxide and Ti/titanium nitride in situ composites to form as a surface layer if no shielding is used due to diffusion of O and N

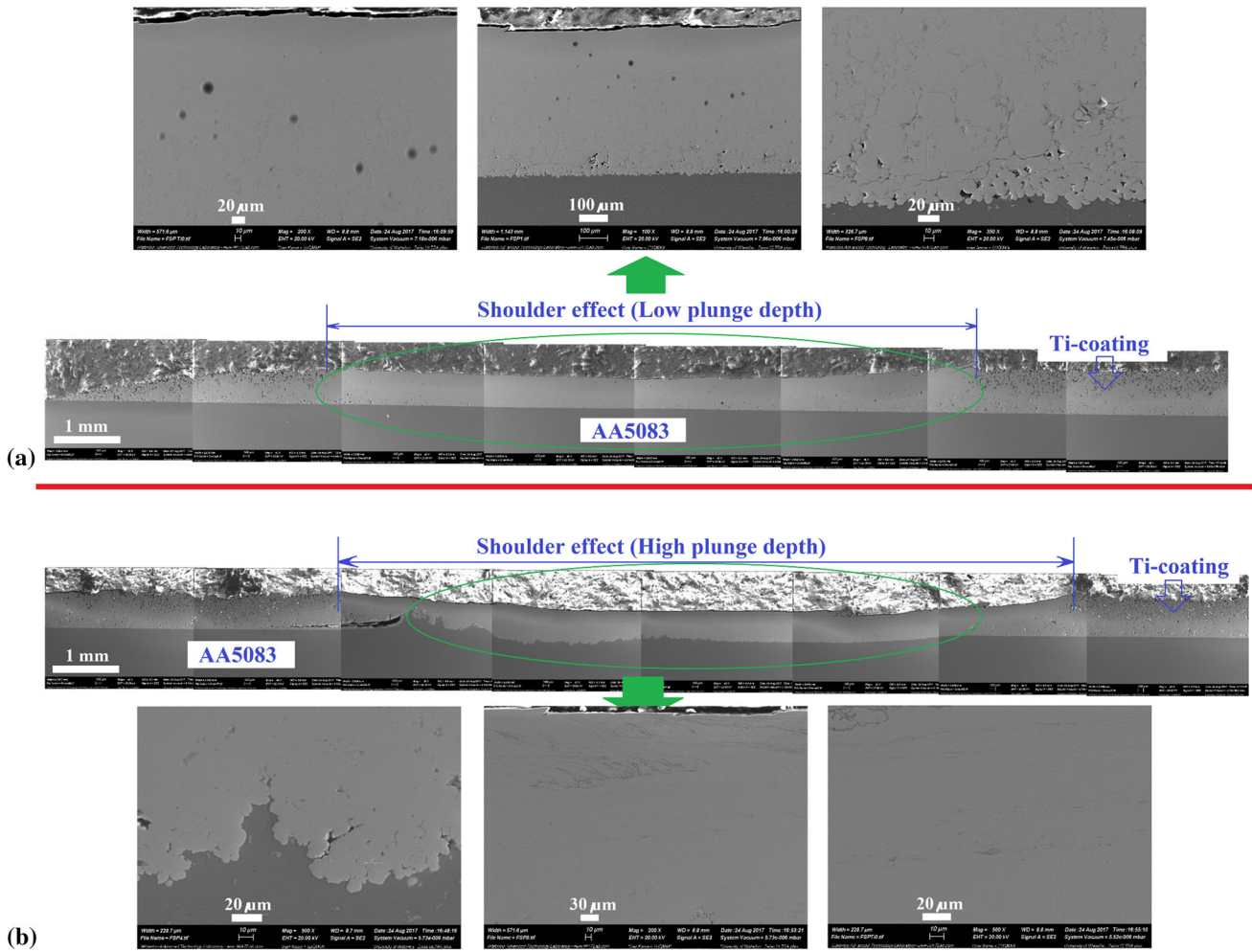
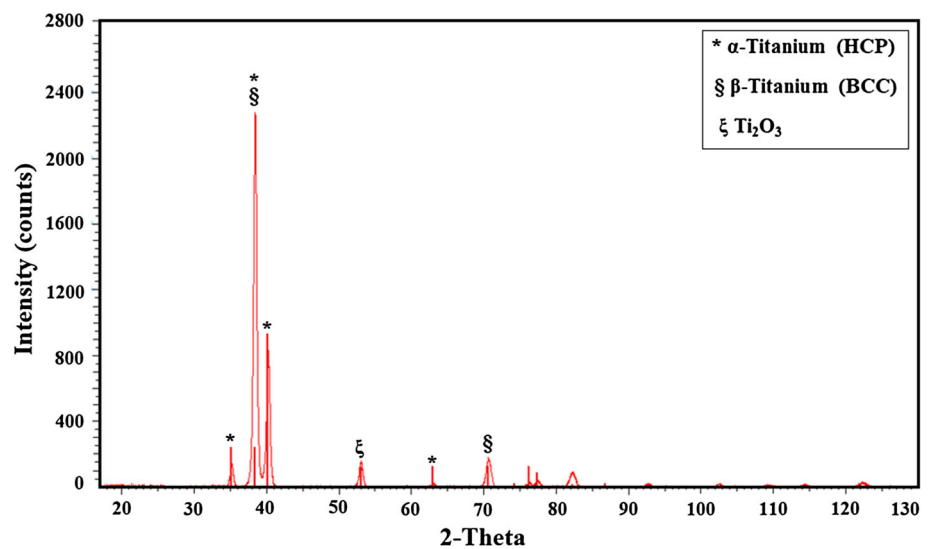


**Fig. 9** Combined maps of FE-SEM images showing the cross-sectional materials flow patterns for the (a) low and (b) high plunge depths friction-stir-modified cold-sprayed coatings. High-

magnification FE-SEM images from the structure of CSed Ti-coatings after FSP modification at low and high plunge depths illustrated as well

**Fig. 10** XRD pattern from the surface of FSP-modified Ti-coating



elements in the solid state. The flow band profiles in Fig. 9(b) are showing the complex material flow pattern for the mixing and stirring of the exposed layer on the surface during FSP treatment. It is obvious that by increasing the tool plunge depth during FSP and subsequently improving the densification and processing peak temperature, the extent of these exothermic reactions can be accelerated, as suggested by a comparison between Fig. 6(c), (d) and (e), (f).

### Micro-hardness profiles across different regions

Figure 11(a) illustrates the Vickers micro-hardness survey for the initial AA5083 alloy substrate. Considering the various hardness measurements, an average hardness value of  $\sim 105$  HV can be reported for the substrate. In Fig. 11(b), a micro-hardness survey from the CSed Ti-coating near the interface is shown. The hardness varies drastically from 75 to 110 HV depending on various locations from the Al/Ti interface, due to the widely varying porosity and complex strain field in the deposited particles. This fluctuation in the hardness results for Ti-coating can be due to presence of pores as well as the complicated strain hardening phenomena during CS deposition of titanium particles by dislocation-related mechanisms (generation, movement, accumulation, and intersection) due to shot-peening effect of particles (Ref 28). Figure 12(a), (b) and (c) shows the micro-hardness maps from advancing side, centerline, and retreating side of the Ti-coating layer after FSP modification with low plunge depth. As seen, closing to the top surface side the amount of indentation micro-hardness is continuously increased. Also, the maximum magnitudes of Vickers hardness are observed in the center region. A hardness value up to  $\sim 700$  HV is measured after FSP modification on the surface layer. In Fig. 13, the hardness results from the same regions of high plunge depth modified sample are reported. Extensive hardening of surface layer caused by FSP treatment is obvious for this specimen as well. A gradual hardness increases from the AA5083 alloy substrate toward the Al/Ti interface and thereafter the top side

of Ti-coating layer can be easily found by considering Fig. 14. Furthermore, the mean indentation Vickers hardness values of different regions (advancing side, center, retreating side, and close to the Al-Ti interface) for the low and high plunge depths FSP-modified CSed coatings are summarized in Table 1 along with their related standard deviations. These results are related to the retreating side of high plunge depth modified sample. These indentation hardness improvements for the CSed Ti-coating after FSP conduction are in good agreement with the observed structural refinement shown in Fig. 6–8. These features can be attributed to the following micro-mechanisms: (1) densification and reducing the fraction of porosities, (2) promoting the grain structural refinements according to the operative dynamic restoration mechanisms, (3) intense plastic deformation and induced further strain hardening effect, (4) martensitic phase transformation, and (5) additional solid-solution strengthening effect because of *N* and *O* elements pickup.

### Conclusions

In the current study, a dense and homogenous Ti-coating layer with superior mechanical properties was deposited on the AA5083 alloy substrate by an innovative hybrid implementation of CS and FSP. The main findings can be summarized as follows:

- Evaluation of CS parameters (pressure and temperature) with satisfactory conditions (203 psi and 500 °C) leads to the formation of a porous ( $\sim 30\%$ , i.e., 30% pores and 70% dense material) Ti-coating layer with a thickness in the range of 800–850  $\mu\text{m}$ .
- By subsequent application of the FSP process on the CSed layer, it is possible to achieve localized surface modification, a fine-grained, uniform, and pore-free structure in the Ti-coating. Material forging, intense plastic deformation, and thermal exposure during FSP cause the significant densification, grain structural refinement, and thereby closing the pores.

**Fig. 11** Micro-hardness maps for the (a) AA5083 alloy substrate and (b) CS-deposited Ti-coating layer

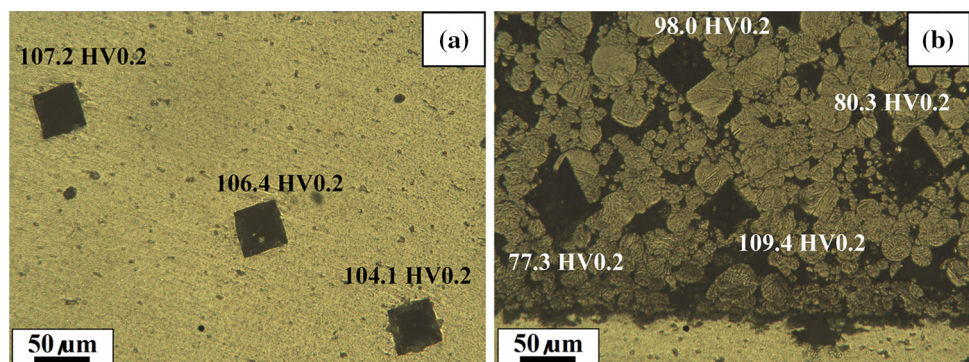


**Fig. 12** Micro-hardness maps for the (a) advancing side, (b) center, and (c) retreating side of low plunge depth modified CSed coating layer by FSP. The modified FSP layer close to surface covered in these images

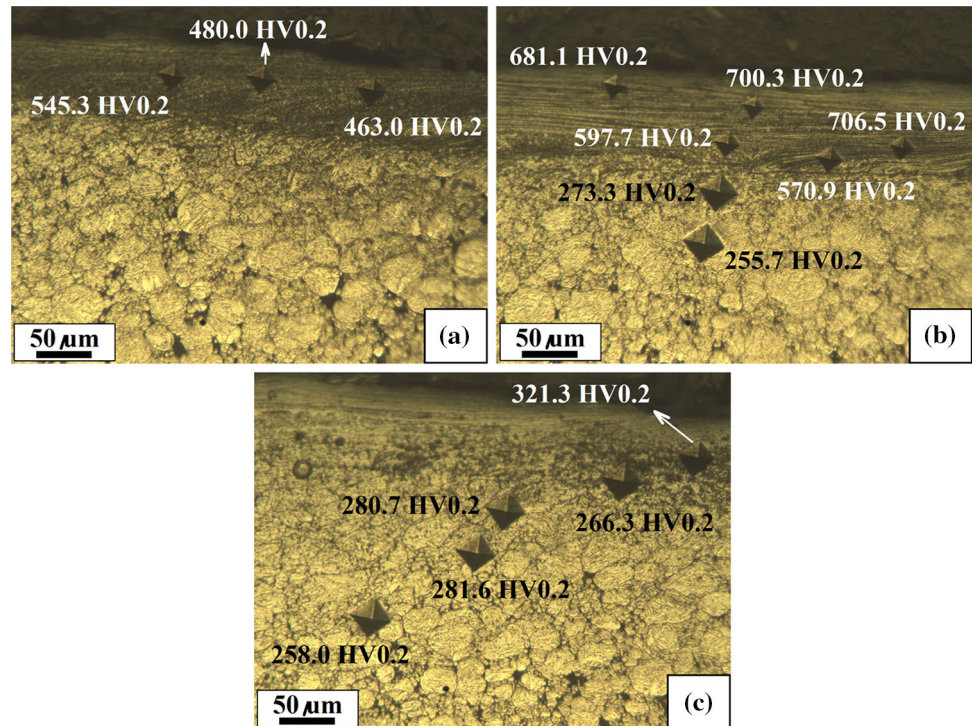
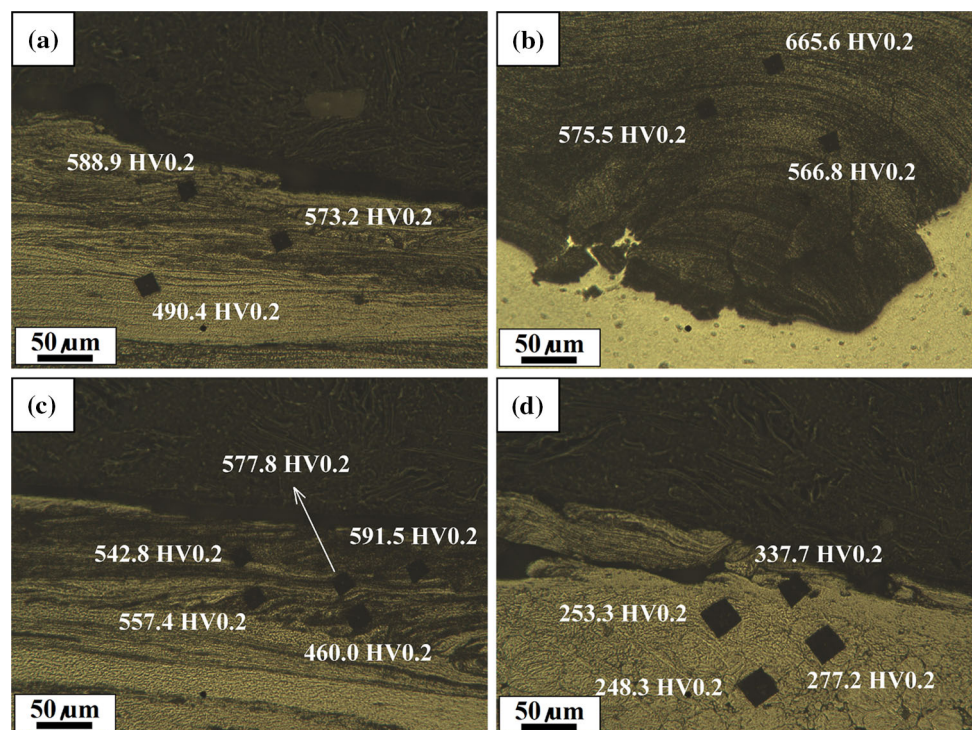


**Fig. 13** Micro-hardness maps for the (a, b) advancing side, (c) center, and (d) retreating side of high plunge depth modified CSed coating layer by FSP



- The material flow within the cold-sprayed coating layer during FSP and subsequent microstructural features were highly dependent on the amount of plunging depth. In the case of low plunge depth sample ( $\sim 0.3$  mm), localized modification was occurred in a layer close to the surface of Ti-coating. However, the

regions close to the interface looks still porous. By increasing the plunge depth (up to  $\sim 0.5$  mm), complete densification is achieved with no porosity, along with severe grain structural refinements ( $< 1$   $\mu\text{m}$ ) and formation of a new wavy morphology at the Al/Ti interface.

**Fig. 14** Micro-hardness gradient across the retreating side of coating layer at high plunge depth from (a) the top layer, (b) in the middle section, and (c) across the interface

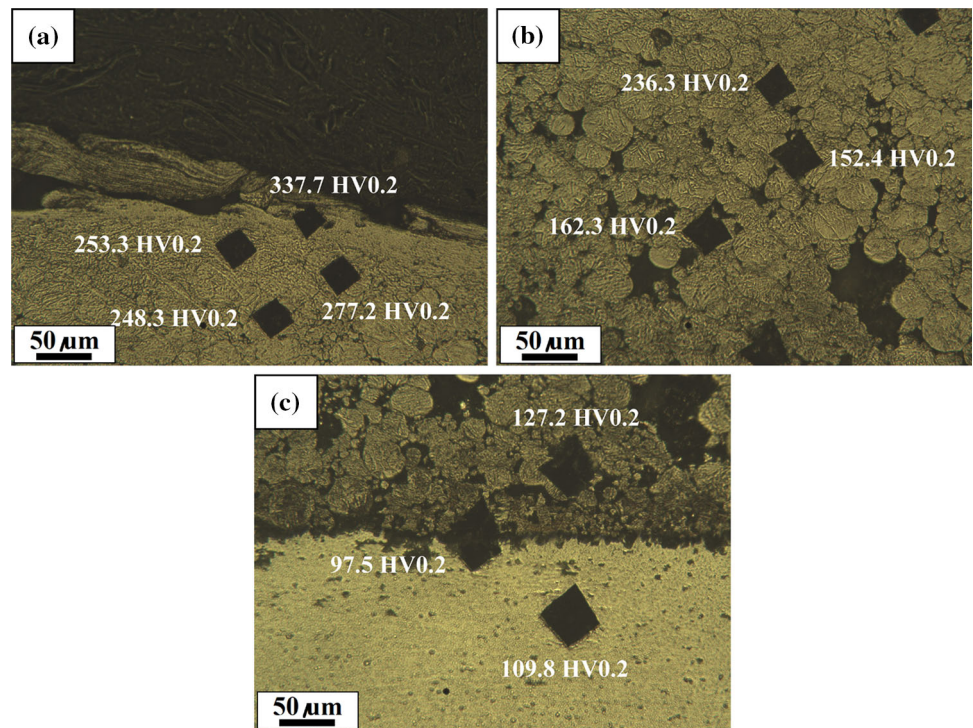


**Table 1** The average indentation Vickers micro-hardness values for different regions across the cold-sprayed and FSP-modified materials

Material	Condition	Parameter	Hardness (HV0.2)					
			Initials/As-sprayed		Modification			
			Substrate	Ti-coating	Advancing side	Center	Retreating side	Close to the interface
AA5083-Ti	FSP	Low plunge depth	105.9 ± 1.3	91.3 ± 18.2	496.1 ± 49.2	651.3 ± 55.2	293.8 ± 27.5	269.9 ± 11.7
AA5083-Ti	FSP	High plunge depth	105.9 ± 1.3	91.3 ± 18.2	576.7 ± 88.9	545.9 ± 45.6	279.1 ± 58.6	169.6 ± 66.8

- FSP has resulted in high Vickers hardness up to the value of ~ 700 HV over the deposited Ti-coating. Formation of this hard layer on the surface after FSP modification can be attributed to the titanium oxidation and nitrogen absorption (to form titanium oxide and titanium nitride phases) during process as well as the coating densification, microstructural refinement, and work-hardening.

**References**

- A. Moridi, S.M. Hassani-Gangaraj, M. Guagliano, and M. Dao, Cold Spray Coating: Review of Material Systems and Future Perspectives, *Surf. Eng.*, 2014, **30**(6), p 369-395. <https://doi.org/10.1179/1743294414y.0000000270>
- H. Assadi, H. Kreye, F. Gärtner, and T. Klassen, Cold Spraying: A Materials Perspective, *Acta Mater.*, 2016, **116**(Supplement C), p 382-407. <https://doi.org/10.1016/j.actamat.2016.06.034>
- T. Schmidt, H. Assadi, F. Gärtner, H. Richter, T. Stoltenhoff, H. Kreye, and T. Klassen, From Particle Acceleration to Impact and Bonding in Cold Spraying, *J. Therm. Spray Technol.*, 2009, **18**(5), p 794. <https://doi.org/10.1007/s11666-009-9357-7>
- C. Borchers, F. Gärtner, T. Stoltenhoff, H. Assadi, and H. Kreye, Microstructural and Macroscopic Properties of Cold Sprayed Copper Coatings, *J. Appl. Phys.*, 2003, **93**(12), p 10064-10070. <https://doi.org/10.1063/1.1573740>
- B. Marzbanrad, H. Jahed, and E. Toyserkani, On the Evolution of Substrate’s Residual Stress During Cold Spray Process: A Parametric Study, *Mater. Des.*, 2018, **138**, p 90-102. <https://doi.org/10.1016/j.matdes.2017.10.062>
- P.D. Eason, S.C. Kennett, T.J. Eden, I. Krull, B. Kowalski, and J.L. Jones, In Situ Observation Of Microstrain Relief in Cold-Sprayed Bulk Copper During Thermal Annealing, *Scr. Mater.*, 2012, **67**(9), p 791-794. <https://doi.org/10.1016/j.scriptamat.2012.07.029>

7. S. Kumar, A. Jyothirmayi, N. Wasekar, and S.V. Joshi, Influence of Annealing on Mechanical and Electrochemical Properties of Cold Sprayed Niobium Coatings, *Surf. Coat. Technol.*, 2016, **296**, p 124-135. <https://doi.org/10.1016/j.surfcoat.2016.04.027>
8. R.S. Mishra, Z.Y. Ma, and I. Charit, Friction Stir Processing: A Novel Technique for Fabrication of Surface Composite, *Mater. Sci. Eng. A*, 2003, **341**(1-2), p 307-310. [https://doi.org/10.1016/S0921-5093\(02\)00199-5](https://doi.org/10.1016/S0921-5093(02)00199-5)
9. R.S. Mishra and Z.Y. Ma, Friction Stir Welding and Processing, *Mater. Sci. Eng. R*, 2005, **50**(1-2), p 1-78. <https://doi.org/10.1016/j.mser.2005.07.001>
10. R. Nandan, T. DebRoy, and H.K.D.H. Bhadeshia, Recent Advances in Friction-Stir Welding: Process, Weldment Structure and Properties, *Prog. Mater. Sci.*, 2008, **53**(6), p 980-1023. <https://doi.org/10.1016/j.pmatsci.2008.05.001>
11. T.R. McNelley, S. Swaminathan, and J.Q. Su, Recrystallization Mechanisms During Friction Stir Welding/Processing of Aluminum Alloys, *Scr. Mater.*, 2008, **58**(5), p 349-354. <https://doi.org/10.1016/j.scriptamat.2007.09.064>
12. F. Khodabakhshi, A. Simchi, A.H. Kokabi, A.P. Gerlich, and M. Nosko, Effects of Stored Strain Energy on Restoration Mechanisms and Texture Components in an Aluminum-Magnesium Alloy Prepared by Friction Stir Processing, *Mater. Sci. Eng. A*, 2015, **642**, p 204-214. <https://doi.org/10.1016/j.msea.2015.07.001>
13. K.J. Hodder, H. Izadi, A.G. McDonald, and A.P. Gerlich, Fabrication of Aluminum-Alumina Metal Matrix Composites via Cold Gas Dynamic Spraying at Low Pressure Followed by Friction Stir Processing, *Mater. Sci. Eng. A*, 2012, **556**, p 114-121. <https://doi.org/10.1016/j.msea.2012.06.066>
14. H. Ashrafizadeh, A. Lopera-Valle, A. McDonald, and A. Gerlich, Effect of Friction-Stir Processing on the Wear Rate of WC-Based MMC Coatings Deposited by Low-Pressure Cold Gas Dynamic Spraying. *Proceedings of the International Thermal Spray Conference*, 2015, p 41-47.
15. C. Huang, W. Li, Z. Zhang, M. Fu, M.P. Planche, H. Liao, and G. Montavon, Modification of a Cold Sprayed SiCp/Al5056 Composite Coating by Friction Stir Processing, *Surf. Coat. Technol.*, 2016, **296**(Supplement C), p 69-75. <https://doi.org/10.1016/j.surfcoat.2016.04.016>
16. C. Huang, W. Li, Z. Zhang, M.P. Planche, H. Liao, and G. Montavon, Effect of Tool Rotation Speed on Microstructure and Microhardness of Friction-Stir-Processed Cold-Sprayed SiCp/Al5056 Composite Coating, *J. Therm. Spray Technol.*, 2016, **25**(7), p 1357-1364. <https://doi.org/10.1007/s11666-016-0441-5>
17. T. Peat, A. Galloway, A. Toumpis, P. McNutt, and N. Iqbal, The Erosion Performance of Cold Spray Deposited Metal Matrix Composite Coatings with Subsequent Friction Stir Processing, *Appl. Surf. Sci.*, 2017, **396**, p 1635-1648. <https://doi.org/10.1016/j.apsusc.2016.10.156>
18. T. Peat, A. Galloway, A. Toumpis, R. Steel, W. Zhu, and N. Iqbal, Enhanced Erosion Performance of Cold Spray Co-deposited AISI316 MMCs Modified by Friction Stir Processing, *Mater. Des.*, 2017, **120**, p 22-35. <https://doi.org/10.1016/j.matdes.2017.01.099>
19. C. Huang, W. Li, Y. Feng, Y. Xie, M.P. Planche, H. Liao, and G. Montavon, Microstructural Evolution and Mechanical Properties Enhancement of a Cold-Sprayed CuZn Alloy Coating with Friction Stir Processing, *Mater. Charact.*, 2017, **125**, p 76-82. <https://doi.org/10.1016/j.matchar.2017.01.027>
20. F. Khodabakhshi, B. Marzbanrad, L.H. Shah, H. Jahed, and A.P. Gerlich, Friction-Stir Processing of a Cold Sprayed AA7075 Coating Layer on the AZ31B Substrate: Structural Homogeneity, Microstructures and Hardness, *Surf. Coat. Technol.*, 2017, **331**(Supplement C), p 116-128. <https://doi.org/10.1016/j.surfcoat.2017.10.060>
21. F. Khodabakhshi, B. Marzbanrad, H. Jahed, and A.P. Gerlich, Interfacial Bonding Mechanisms Between Aluminum and Titanium During Cold Gas Spraying Followed by Friction-Stir Modification, *Appl. Surf. Sci.*, 2018, **462**, p 739-752. <https://doi.org/10.1016/j.apsusc.2018.08.156>
22. ASTM E384-17: Standard Test Method for Microindentation Hardness of Materials.
23. M. Faizan-Ur-Rab, S.H. Zahiri, S.H. Masood, T.D. Phan, M. Jahedi, and R. Nagarajah, Application of a Holistic 3D Model to Estimate State of Cold Spray Titanium Particles, *Mater. Des.*, 2016, **89**, p 1227-1241. <https://doi.org/10.1016/j.matdes.2015.10.075>
24. F. Khodabakhshi, A. Simchi, A.H. Kokabi, P. Švec, F. Šimančík, and A.P. Gerlich, Effects of Nanometric Inclusions on the Microstructural Characteristics and Strengthening of a Friction-Stir Processed Aluminum-Magnesium Alloy, *Mater. Sci. Eng. A*, 2015, **642**, p 215-229. <https://doi.org/10.1016/j.msea.2015.06.081>
25. A. Shamsipur, S.F. Kashani-Bozorg, and A. Zarei-Hanzaki, Production of In Situ Hard Ti/TiN Composite Surface Layers on CP-Ti Using Reactive Friction Stir Processing Under Nitrogen Environment, *Surf. Coat. Technol.*, 2013, **218**, p 62-70. <https://doi.org/10.1016/j.surfcoat.2012.12.028>
26. P.D. Edwards and M. Ramulu, Investigation of Microstructure, Surface and Subsurface Characteristics in Titanium Alloy Friction Stir Welds of Varied Thicknesses, *Sci. Technol. Weld. Join.*, 2009, **14**(5), p 476-483. <https://doi.org/10.1179/136217109X425838>
27. A. Shamsipur, S.F. Kashani-Bozorg, and A. Zarei-Hanzaki, The Effects of Friction-Stir Process Parameters on the Fabrication of Ti/SiC Nano-composite Surface Layer, *Surf. Coat. Technol.*, 2011, **206**(6), p 1372-1381. <https://doi.org/10.1016/j.surfcoat.2011.08.065>
28. S.B. Dayani, S.K. Shaha, R. Ghelichi, J.F. Wang, and H. Jahed, The Impact of AA7075 Cold Spray Coating on the Fatigue Life of AZ31B Cast Alloy, *Surf. Coat. Technol.*, 2018, **337**, p 150-158. <https://doi.org/10.1016/j.surfcoat.2018.01.008>

**Publisher's Note** Springer Nature remains neutral with regard to jurisdictional claims in published maps and institutional affiliations.